PHYSICAL REVIEW B VOLUME 9, NUMBER 7 1 APRIL 1974

Depth profiling of ^{3}He and ^{2}H in solids using the ^{3}He(d, p) ^{4}He resonance*

P. P. Pronko
Argonne National Laboratory, Argonne, Illinois 60439

J. G. Pronko
Lockheed Palo Alto Research Laboratory, Palo Alto, California 94304

(Received 17 September 1973)

An *in situ* nondestructive probe for measuring the concentration and distribution of helium and hydrogen isotopes in near-surface layers of solids is described. The technique makes use of the ^{3}He$(d, p)^4$He resonant nuclear reaction. A probing beam of deuterons is used to analyze for ^{3}He (a ^{3}He beam may be used to analyze for deuterium). Stopping-power effects control deceleration of the probing beam and bring the energy into the resonance window. Integration of the proton yield at a given beam energy determines the quantity of ^{3}He or deuterium at the depth associated with the probe upon entering resonance. Spatial resolution of the method is defined by the 350-keV full width at half-maximum for the resonance cross section. Examples of ion-implanted ^{3}He distributions in niobium are presented along with a discussion of mathematical-deconvolution and oblique-incidence resolution-enhancement techniques. Normal-incidence resolution is ~ 3 μm and can be improved using mathematical deconvolution. Oblique incidence (75° from the normal to the surface) in conjunction with deconvolution, yields adjacent-peak-position resolution to nominal values of 3000 Å by artificially broadening the distribution of ^{3}He without changing the resolution function. Small-angle multiple scattering and energy straggling of the probing beam under these conditions introduces a limit on peak-width resolution of about 6000 Å. Differential cross sections for the reaction range between 50 and 80 mb/sr (depending on observation angle), which results in minimum observable concentrations of about 10 ppm. The method has technical value for analyzing potential problems associated with the implanation of helium in materials that may be used for the primary containment wall of controlled-fusion reactors.

I. INTRODUCTION

The characterization of solids implanted with helium or hydrogen is of concern to a variety of fields. The performance of breeder reactors and controlled-thermonuclear-fusion reactors will be affected by the presence of these elements, which will be injected into the metallic components of the reaction chambers. Solar-wind effects on solids such as moon rocks and space vehicles are associated with the injection of these gases. Recently, work on deuterium-injected palladium has resulted in significant changes in its superconducting characteristics. Energetic helium and hydrogen beams are used to produce damage patterns in laser light pipes that modify the refractive index and allow selective handling of laser beams. Radiation-enhanced diffusion in semiconductors is often achieved by bombarding with helium or hydrogen beams. Information on the location and concentration of these injected gases is, therefore, of interest.

Measurements of the distribution of ion-implanted helium and hydrogen in solids has progressed less rapidly than similar measurements on the distributions of heavy ions. One reason has been the lack of simple techniques for direct observation of such distributions. Light ions do not readily lend themselves to radioactive-tracer profiling, since suitable active isotopes are not available. Other direct techniques such as elastic scattering restrict sample geometries to thin films and thereby introduce the complexities associated with such films.[1]

These circumstances have led us to investigate the usefulness of the ^{3}He$(d, p)^4$He resonant nuclear reaction as a profiling technique. The concept of using resonant reactions for depth profiling has been applied with good success by other workers[2–4]; however, the problems associated with a broad yield curve, as is found in the deuterium-^{3}He reaction, have never been adequately assessed. This particular reaction is attractive since many accelerators have radio-frequency ion sources that can readily produce deuterium or helium beams in the energy range of 0.25 to 2 MeV. The reaction ^{3}He$(d, p)^4$He can be applied to the profiling of either helium or deuterium; however, the resonance width (~ 350 keV) and high-energy tail present problems in terms of ultimate special resolution. The primary purpose of the present study was to examine the potential of this method and to determine whether resolution enhancement could be achieved through geometrical and mathematical methods. Experimental results will be presented for helium profiles in niobium, and appropriate comments will be added on the application to deuterium distributions.

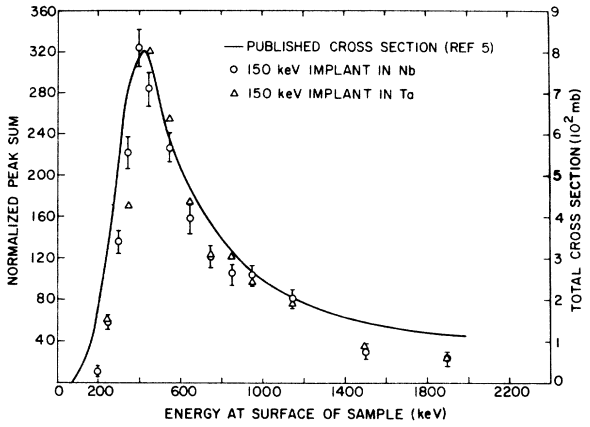

FIG. 1. Proton yield data for ^{3}He$(d,p)^4$He reaction plotted in laboratory coordinates. The curve is published cross section for gas target. The two implants are sufficiently narrow to reproduce the gas-target results.

II. CHARACTERISTICS OF THE ^{3}He$(d,p)^4$He REACTION

The published proton yield curve[5] for the reaction is presented in Fig. 1. The peak appears at an energy of 430 keV with a full width at half-maximum of 350 keV. The resonance tail extends out to the range of 2 MeV.

The Q value for the reaction is 18.341 MeV. At a 150° scattering angle the proton energy is 13.64 MeV, which is well above the particle energies of competing reactions. The concentration of ^{3}He at any particular depth will be determined by the sum of proton counts observed at a fixed angle. Table I lists the energy associated with reaction products of interest from deuterons impinging on ^{3}He, ^{12}C, and ^{16}O as a function of observation angle. Reaction-product energies for the inverse case where ^{3}He is the incident beam are also given. Information on carbon and oxygen are presented as a calibration aid, since these elements are often present on the surface of a sample and tend to be useful for a calibration of energy.

The differential cross sections for analyzing with a deuteron or ^{3}He beam are presented in Fig. 2. It can be seen that the yield is 25% lower in the back angles; however, with bulk specimens these are the only angles that can be used. Differential cross sections of 60 mb/sr will result in minimum observable concentrations of 10–100-ppm ^{3}He depending on beam-exposure requirements.

III. EXPERIMENTAL METHOD

A. Apparatus

Polycrystalline niobium specimens were implanted with ^{3}He using various facilities. For low-energy implants (150 keV), the heavy-ion accelerator at the Materials Science Division of Argonne National Laboratory was used. The 3-MeV Stanford Van de Graaff and the Lockheed Van de Graaff were used for implants in the 0.5- to 3-MeV range. A broad region was implanted using an electrostatically swept beam. Doses were in the range of 10^{14} to 10^{16} ions/cm^2.

Analysis of the implanted samples was performed on the Lockheed 3-MeV Van de Graaff. A schematic diagram of the experimental setup is given in Fig. 3. Beam energies between 200 keV and 3 MeV were employed. The sample, while mounted in the target holder, could be rotated so that the beam was incident at $10° \leq \theta \leq 90°$ to the surface.

Current integration was done by electrostatic-charge collection. The suppression of secondary electrons was found to be a crucial factor in obtaining correct results on reaction yields as a function of energy. The secondary-electron yield varies as a function of beam energy and, if the effect of these secondary electrons is not totally suppressed, gross errors in the resultant ^{3}He profiles will occur. A simple negatively biased (−300 V) suppressor plate in front of an unbiased target was found inadequate for the higher (> 1 MeV)

TABLE I. Proton reaction-product energies (MeV).

	E_d = 430 keV			$E_{^3\mathrm{He}}$ = 645 keV		
θ_p (deg)	^{3}He$(d,p)^4$He	^{12}C$(d,p)^{13}$C	O$^{16}(d,p)$O^{17}	D$(^3$He$,p)^4$He	^{12}C$(^3$He$,p)^{14}$N	^{16}O$(^3$He$,p)^{18}$F
0	16.34	3.61	2.32	17.10	5.36	2.67
30	16.13	3.51	2.30	16.77	5.30	2.64
60	15.57	3.24	2.25	15.90	5.14	2.55
90	14.83	2.90	2.17	14.79	4.93	2.43
120	14.13	2.60	2.09	13.75	4.73	2.32
150	13.64	2.40	2.04	13.04	4.58	2.24
180	13.46	2.33	2.02	12.79	4.53	2.21
	Q_0 = 18.35	3.42	1.92	18.35	4.78	2.033

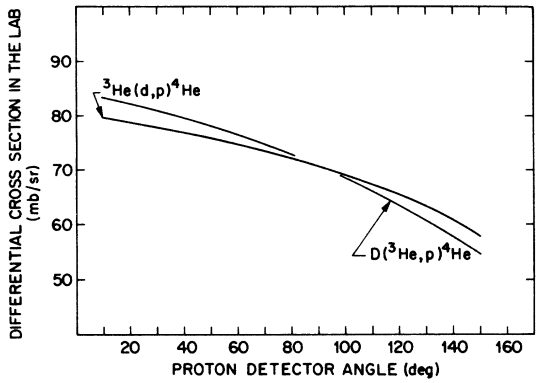

FIG. 2. Differential laboratory cross sections ($d\sigma/d\Omega$ at resonance) for the reactions ^{3}He(d,p)^{4}He and D(^{3}He, p) ^{4}He as a function of proton detector angle. This information is required for extracting absolute concentrations of implanted ^{3}He or deuterium.

energy probes. This simple arrangement did seem to function satisfactorily for lower energies; however, its general use introduces unnecessary risk of error. The biasing technique that was used is shown in Fig. 3. The final analyzing-beam collimator, with a diameter (~ 1 mm) much smaller than the implanted region, was maintained at +300 V. Thus, the collimator, in addition to defining the beam, will separate and collect electrons drifting with the deuteron beam as well as recapturing electrons ejected from the edges of its aperture. A suppression electron shield in the form of a cylinder, with a cap on top, enclosed the sample. An entrance port for the probing beam and an exit port for the reaction protons were the only openings around the cylinder. This suppression shield was maintained at −300 V to return secondary electrons to the specimen. The specimen was biased +300 V to enhance its collection efficiency for secondary electrons. The current carried by the protons (i.e., positive charge leaving the target) is negligible in comparison to the beam current that strikes the target. Thus, errors in current integration due to loss of protons, backscattered deuterons, and secondary electrons ejected from the suppression cylinder can be neglected.

The 13-MeV reaction-product protons were observed, at 145° to the incoming beam, with a silicon detector that had a depletion depth of 3000 μm and a 2-μA leakage current. The detector was collimated with a 6-mm-diam aperture and positioned a distance of 34 mm from the target to give a detector solid angle of 0.0244 sr. The detector face was covered with a 0.0012-in. aluminum foil to prevent flooding by backscattered deuterons.

B. Extracting distributions

Deceleration of the deuteron probing beam occurs primarily from electronic stopping. Consecutive small-angle scattering from nuclear and electronic collisions will broaden the beam into a cone of angle ϕ and also introduce energy straggling. These two effects (beam broadening and straggling) impose certain limitations on the ultimate accuracy of the observed distributions. They are discussed in more detail below.

For helium located at or near the surface, the energy of deuteron incidence, for which the proton reaction yield will be a maximum, is at the peak of the cross-section curve (430 keV) in Fig. 1. Contained in the figure are data points taken for 150-keV implants of 10^{15} ^{3}He/cm^2 in niobium and tantalum. These injection conditions result in distributions that are sufficiently narrow and near the surface to reproduce the gas-target results. For helium implanted deeper in the material, the incident-deuteron probing energy must be raised to a higher value such that the energy of resonance is reached simultaneously with the passage of the deuterons through the region where the helium is deposited. The host material between the surface and the depth of the helium acts to decelerate the deuterons to the resonance energy. Thus, a plot

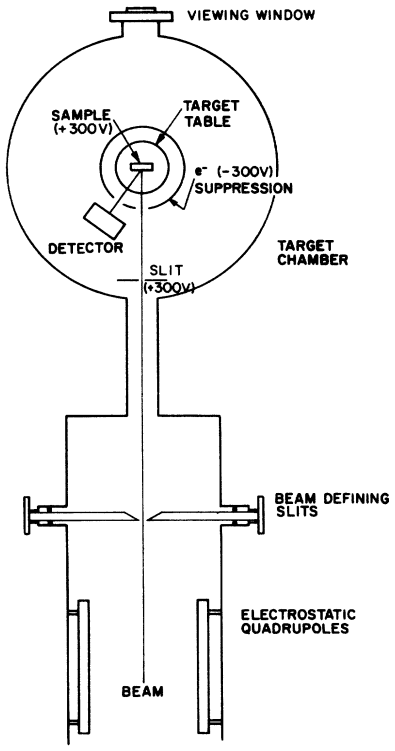

FIG. 3. Schematic diagram of experimental system.

of integrated proton yield versus incident deuteron energy (i.e., energy at the surface) results in the raw data for the depth distribution of helium. This information must undergo several corrections before it can be read as the true distribution in depth.

The following steps are used to obtain the experimental distribution that is reasonably close to the true distribution: (i) Convert the deuteron probing energy to range along the path prior to entering resonance. (ii) Correct the range along the path to the projected range. (iii) Take advantage of oblique-incidence resolution enhancement, if necessary. (iv) Deconvolute the resolution function from the observed distribution.

C. Distance to resonance and projected range

The stopping power (dE/dx) determines the distance a high-energy-deuteron beam will penetrate before reaching resonance. The total distance traveled is

$$D_{\text{total}} = \int_{E_0}^{E_x} dE \Big/ \left(\frac{dE}{dx}\right) .$$

Stopping-power information is available from several sets of published tables. We have used the detailed compilation of Williamson, Boujot, and Picard (WBP) for the range along the path of ^{3}He and deuterium in niobium.[6] The distance to resonance is given as $R = R_E - R_{(0.43)}$, where R is the total path traveled before reaching resonance, R_E is the total range for a particle with energy E, and $R_{(0.43)}$ is the total range for a particle with energy 0.43 MeV.

The case of projected ranges for light particles in the low-MeV category has been treated by Schiott.[7] His approach is an extension of the Lindhard, Scharff, and Schiott[8] (LSS) theory for heavy particles. Projected ranges for ^{3}He and deuterium in niobium are presented in Fig. 4. These curves were obtained by using total range from WBP and by applying Schiott's corrections for projected range. Figure 5 gives the projected distance to resonance for implanted ^{3}He as a function of deuteron-beam energy at the surface as well as projected distance to resonance for implanted deuterium as a function of ^{3}He energy at the surface.

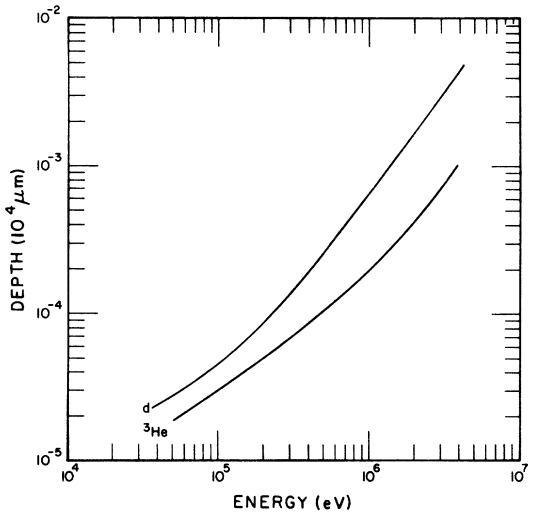

FIG. 4. Projected ranges of ^{3}He and deuterium in niobium. Total range taken from Ref. 6 and projected corrections from Ref. 7.

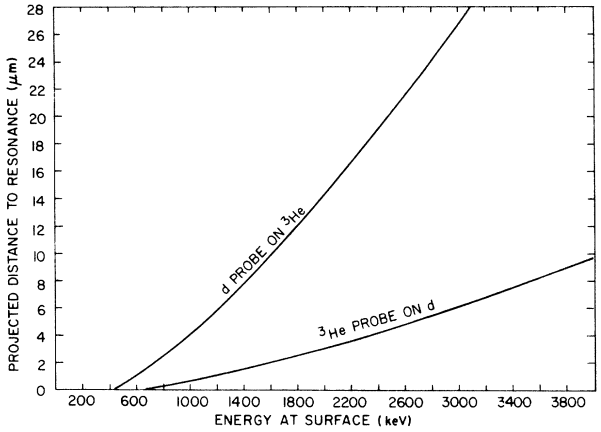

FIG. 5. Projected distance to resonance for implanted ^{3}He as a function of deuteron beam energy (laboratory) at the surface (as well as the inverse case).

D. Oblique incidence

As mentioned earlier, resolution-enhancement techniques are required for dealing with the rather broad resonance function that will be folded into the real distribution. To achieve maximum resolution, a combination of oblique incidence and mathematical deconvolution are required.

The value of oblique incidence is illustrated in Fig. 6. For vertical incidence, the resolution is equivalent to the half-width of the yield function divided by the stopping power and is on the order of 3.5 μm for materials in the mass range of 100 amu. However, by directing the beam at an oblique angle with respect to the surface, an improvement in resolution occurs because of an artificial broadening in the ^{3}He distribution without an equivalent change in the resolution function. Thus, the depth is $d = L\sin\theta$, where θ is the angle between the surface and the probing beam, and the path length of the probing beam in the material is given by L. The vertical depth resolution under oblique incidence conditions is, therefore,

$$\delta d = \delta L \sin\theta + L\cos\theta\delta\theta. \qquad (1)$$

The first term describes the effect of artificially broadening the distribution. The second term describes the resolution loss due to beam divergence. The half-width of the yield curve defines δL, whereas the cone subtended through beam divergence defines $\delta\theta$. In the limit of $\theta = 90°$ the second term in Eq. (1) is zero and $\delta d = \delta L$.

Proper collimation can keep the beam divergence to negligible values prior to its striking the surface ($< 0.1°$); however, upon entering the crystal, small-angle multiple scattering will cause an angular spread in the beam that is estimated to reach $\sim 10°$ in micron depths.[9] Thus, application of the oblique-incidence technique requires a balance between the resolution improvement afforded by the first term in Eq. (1) and the degradation contributed by multiple scattering introduced in the second term. The optimum angle of incidence appears to be on the order of 15°–20° with respect to the surface (i.e., 70°–75° to the normal) when probing to less than 10 μm of vertical depth.

A procedural method of dealing with oblique incidence is to obtain the experimental oblique distribution, project it to vertical depth and deconvolute with a resolution function that, under these conditions, must be correspondingly narrowed by the same $\sin\theta$ correction. The effective narrowing of the resolution function for 15° incidence is shown in Fig. 7. As will be discussed in Sec. IV, this approach has two advantages. First, it yields a more realistic distribution in terms of the raw data and, second, it allows for a standardized vertical-depth deconvolution procedure. The alternate method is to use the normal resolution function of Fig. 1 to deconvolute the unprojected oblique data. We found the former technique to be easier; however, both methods give the same result.

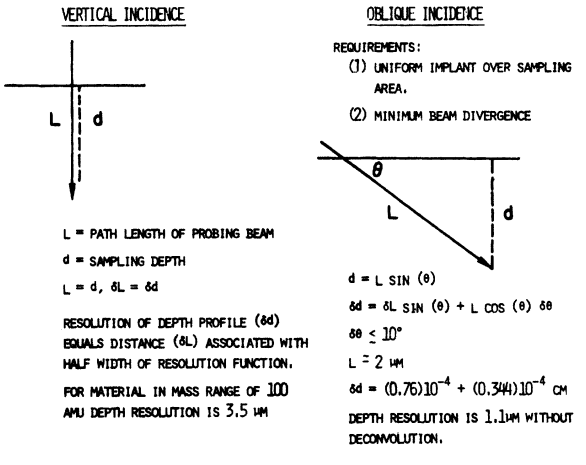

FIG. 6. Geometry used for oblique-incidence probe.

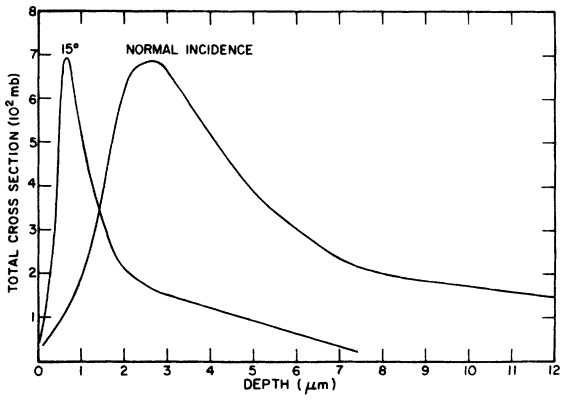

FIG. 7. Effective narrowing of resonance function using 15° oblique incidence.

E. Deconvolution

Mathematical deconvolution of the resonance function from the observed distribution, when used in conjunction with oblique incidence, yields maximum resolution enhancement. Several methods for deconvolution are possible; the choice is dictated by the requirements of the problem and the shape of the distribution.

A rather complete description of the Fourier-transform deconvolution process using fast-Fourier-transform computer techniques has recently been given for the analysis of depth distributions.[10] Other methods are also possible.

We have used the Fourier-transform method for some of our deconvolution analyses, but find it less amenable than a forward process of convolution with trial distribution functions. In general, one needs only three or four trial distributions to arrive at the correct shape, and the computer time involved is usually trivial. Likewise, forward convolution with trial functions can be performed rather easily with a desk calculator and graphic analysis.

Folding of the resolution function with the real distribution is given by the standard convolution integral:

$$\frac{dR(x')}{d\Omega} = R_0 \int_{x_1}^{x_2} N(x)\, \frac{d\sigma(x-x')}{d\Omega}\, dx ,$$

where $dR(x')/d\Omega$ is the observed counts per detector solid angle at a fixed energy, R_0 is the total number of incident particles in the probing beam, $N(x)$ is the true distribution of ^{3}He, and $d\sigma(x-x')/d\Omega$ is the differential cross section for the reaction as a function of depth x when the peak of the reaction cross section is positioned at x'. (Changing the energy of the beam moves x'.) The limits of integration x_1 to x_2 define the practical extremities

of the true distribution $N(x)$. It is the true distribution that is approximated through various trial functions in our analysis.

IV. OBSERVATIONS AND RESULTS

Samples were prepared using multiple-energy implants so that the yield from distributions containing a variety of shapes could be examined. One specimen was implanted at four energies using dissimilar doses. The sequence was arranged in such a way as to have a large central peak with smaller satellite peaks on either side. The central peak was produced with a ^{3}He doses of 10^{16} cm^{-2} at 2 MeV. Two lower-energy peaks were established with 2×10^{15} cm^{-2} at 1.6 MeV and 3.0×10^{15} cm^{-2} at 0.75 MeV. A higher-energy peak was introduced with a 1.5×10^{15} cm^{-2} at 2.5 MeV. Figure 8 shows the results of normal-incidence analysis for this distribution. In Fig. 8(a), the raw data is plotted on an energy scale, and, in Fig. 8(b), the same distribution is converted to a depth scale using Fig. 5. The narrowing of the data, when plotted on an energy scale, as compared to the depth scale, is a consequence of the nonlinearity of the energy to depth conversion (Fig. 5). The dominance of the high-dose 2-MeV implant is clearly seen with the lower-dose implants being almost totally submerged in the yield from this principal peak. The shape of this peak is nearly the same as the resonance curve [Fig. 8(b)]. The insensitivity of the analysis to these lower-dose peaks is a consequence of the width and shape of the resonance yield curve. The depth expected from theory for the 2-MeV implant is 3.65 μm, which results in a shift of the resonance energy to 0.935 MeV. The peak is observed at 0.95 MeV, which corresponds to a depth of 3.8 μm, in fair agreement with theory. Deconvolution of this profile was not attempted since it so closely resembles the resolution function. The solid curve in Fig. 8(b) is just the resolution function which has been overlaid on the data set to demonstrate this similarity. Some occasional points deviate beyond statistical fluctuations in the regions where the low-dose implants should appear; however efforts to fit a convoluted curve to this data set would not yield much information since only one or two points are available for identifying the satellite peaks.

A different sample was implanted sequentially at 1 and 2 MeV with equal doses of 2×10^{16} cm^{-2} and analyzed with both normal and oblique incidence. The results of the analyses are shown in Fig. 9. In this case, a double peak is detected under normal incidence; however, the symmetry does not correspond to the expected LSS double-Gaussian approximation to the profile. In fact, the low-energy implant merely appears as a shoulder on the near-surface side of the distribution. This effect is caused by the broadness of the resonance shape, which results in nearly twice the counts on the high-energy peak.

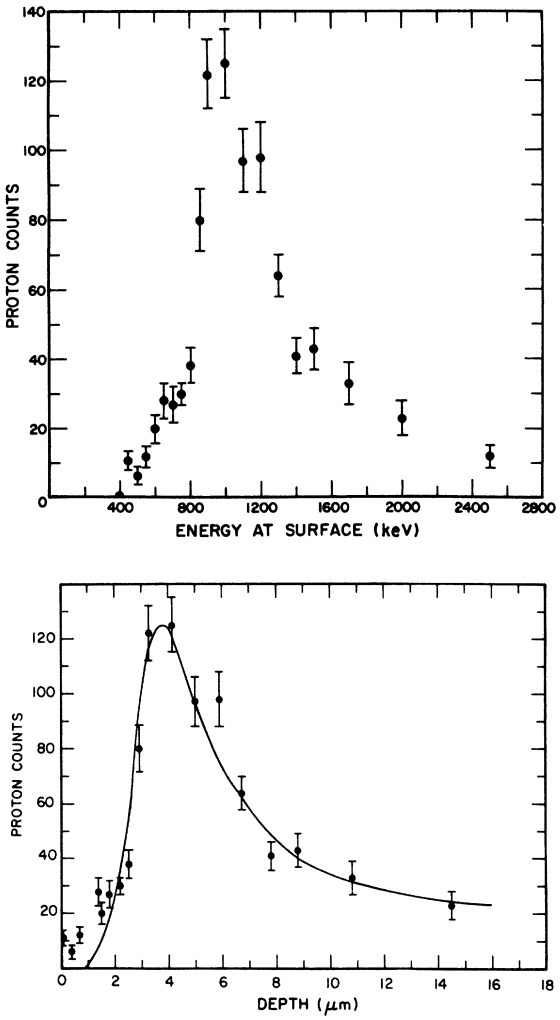

FIG. 8. Normal-incidence probe of multiple energy ^{3}He implant of 1.5×10^{15} cm^{-2} at 2.5 MeV, 10^{16} cm^{-2} at 2 MeV, 2×10^{15} cm^{-2} at 1.6 MeV, and 3×10^{15} cm^{-2} at 0.75 MeV. [(a) is plotted on an energy scale and (b) on a depth scale.] The solid line in (b) is just the resonance function of Fig. 1.

The results of profiling this same double-energy implant at 15° to the surface are also presented in Fig. 9. The solid circles are the data points taken along the oblique path of the beam. A simple $\sin\theta$ correction converts the 15° data to a vertical-depth profile; however, some words of caution about the interpretation of Fig. 9 are required. First, the use of vertical and oblique incidence will produce two quite different profiles simply because of the geometric difference in how they are obtained. However, a more significant differ-

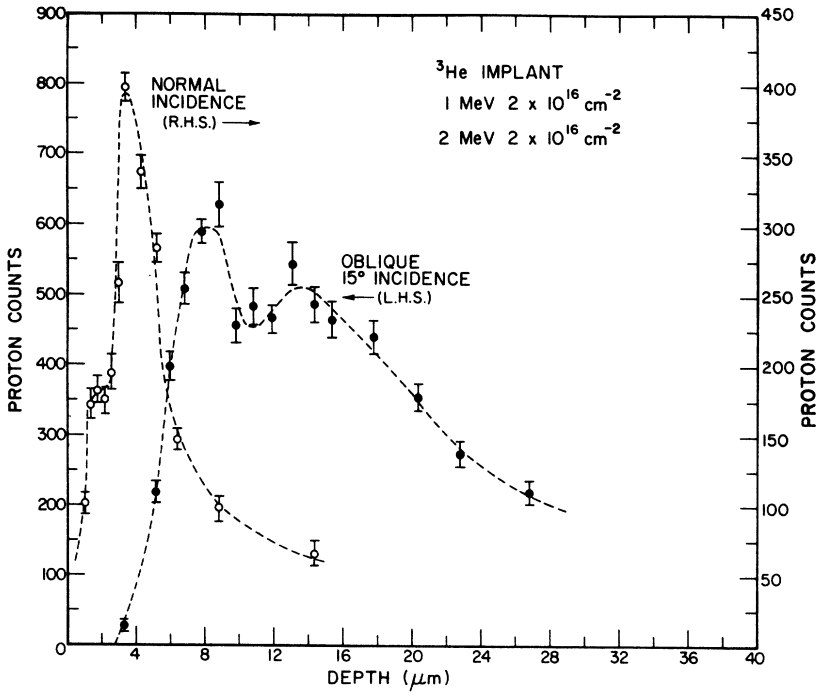

FIG. 9. Data obtained from normal-incidence probe (open circles) of a double-energy ^{3}He implant (2×10^{16} cm^{-2} at 1 MeV and 2×10^{16} cm^{-2} at 2.5 MeV) compared with oblique-(15° from surface) incidence probe. Dashed curves are used only as an aid in connecting data points.

ence occurs as a result of the resolution function of the analyzing beam being folded with two dissimilar depth-dependent concentrations as seen by the probing beam. The result is that the two curves of Fig. 9 must be considered in terms of the convoluting process of Eq. (2) as well as the geometric difference. It is for this reason that the total number of counts under each of the curves differs as well as the fact that if the oblique-incidence curve were given in the $\sin\theta$ correction it would not reproduce the vertical-incidence curve. The real utility of the oblique-incidence method comes from these differences.

Figure 10 gives the experimental points after the $\sin\theta$ correction has been made. The double-Gaussian distribution is beginning to emerge in the experimental data; however, it is still distorted by the resolution-function folding. Since the data have been corrected to vertical incidence, the 15° resolution function of Fig. 7 can be used to unfold the true distribution according to Eq. (2). Performing the deconvolution we arrived at the two Gaussians of Fig. 10 for describing the true distribution. When folded with the 15° resolution function, they yield the solid line in Fig. 10, which gives rather good agreement with the experimental points. The normalization is done such that the sum of the areas under the Gaussians equals the total area under the solid curve. The area under each Gaussian, when calculated from the left-hand differential concentration scale (which is based on 59-mb/sr maximum cross section[11]), reproduces the total implanted dose of 2×10^{16} cm^{-2} within 5% for each implant. The peak positions of 1.8 and 3.8 μm are within 10 and 15% of theory. The Gaussian half-widths of 0.9 and 1.45 μm are 49 and 62% broader than expected from theory. In arriving at these results no corrections were made for the angular spread in the beam. The broadened half-widths may be an artifact caused by beam broadening under oblique analysis. Alternatively the effect could be caused by some diffusion of the helium be-

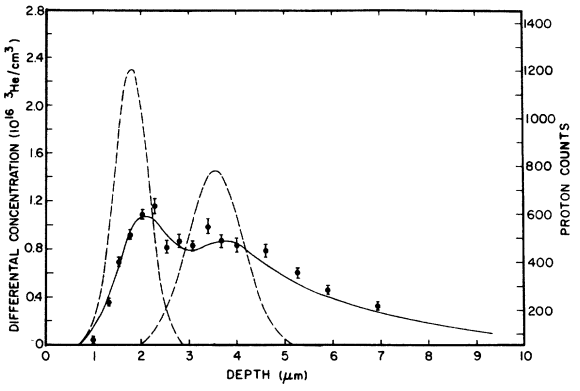

FIG. 10. Oblique-incidence data of Fig. 9 projected into a vertical depth profile. The double Gaussian (dashed curves) represents the distribution chosen for the helium profile. Solid curve is resultant convoluted yield generated from the double Gaussian using the oblique-incidence resolution function.

fore stabilizing in permanent traps.

In order to check the consistency of our results, the two Gaussians, as obtained from oblique analysis, were used with the unprojected resolution function of Fig. 7 to predict the shape of the normal-incidence-data curve. Rather good agreement was obtained (Fig. 11) with the normal-incidence-data points; however, the general degradation of resolution for normal incidence results in a somewhat poorer fit than was found in Fig. 10. The general shape agreement, however, is quite good and no further improvement to the normal-incidence-data fit could be made by adjusting the widths or locations of the Gaussians. It is, therefore, concluded that the oblique and normal incidence data are consistent and the Gaussian distributions obtained from the oblique analysis are the best representation available from this work for the true distribution of implanted helium at energies of 1 and 2 MeV in niobium. The agreement between oblique- and normal-incidence analysis suggests that beam broadening in the 15° probe was not a serious problem.

V. DISCUSSION

The results of the previous section indicate that, unless the distribution of helium is greater than about 3 or 4 μm, it is necessary to use resolution-enhancement techniques for obtaining detailed information about the helium distributions. These consist of oblique-incidence probing and mathematical deconvolution.

Although the use of oblique incidence can, in principle, produce arbitrary narrowing of the resonance function, it is limited by energy straggling and beam broadening due to small-angle multiple scattering. Calculation of the expected cone subtended by the analyzing beam[9] indicates that one can expect ~10° beam broadening in micron depths. Such broadening will degrade the resolution by about 3000 Å (see Fig. 6). In addition, energy straggling can become significant for large energy losses. Calculation[12] of the energy straggling of a deuterium beam starting at 2 MeV and decelerating to 430 keV results in a predicted range straggling of 5000 Å at resonance. Combining these effects in quadrature gives a resolution limit of 6100 Å. It is very likely that these effects are responsible for the approximately 50%-broadened half-widths of the double Gaussians in Fig. 10. In spite of these problems, it is observed that the relative position of two adjacent peaks, with peak-to-valley ratios of 0.5, can be located to better than 3000 Å with respect to each other when using oblique incidence and deconvolution.

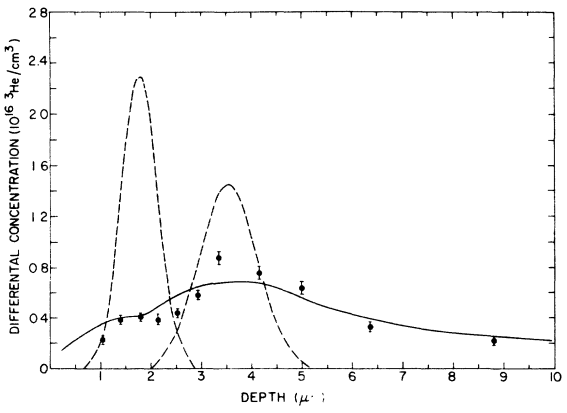

FIG. 11. Normal-incidence data of Fig. 9. The solid curve is resultant convoluted yield generated by the double Gaussians (dashed curves) from Fig. 10 using the normal-incidence resolution function.

The above results indicate that multiple scattering could seriously limit resolution enhancements obtained from oblique incidence. It is helpful, therefore, to qualify the concept of "resolution enhancement." Actually, two factors are involved; one is shape improvement and the other is improved limits on peak-to-valley separation of adjacent peaks. For narrow distributions, the oblique incidence will always result in improvements of the observed shape of the distribution. Multiple scattering will introduce limitations of the observable peak-to-valley separations or, in the case of a a smooth distribution, the half-width and apparent elongation of the far side of the distribution.

Experiments should be performed in which the concentration of ^{3}He is measured as a function of surface removal to independently determine the accuracy of the nuclear-reaction method for observing these distributions. Information concerning the effects of multiple scattering could be extracted from such studies and compared with results from thin-foil scattering experiments.

Multiple-scattering theory as it now exists is not really suited to calculations where large energy losses are associated with the beam broadening.[9,13] Therefore, theoretical calculations can only be used as a guide to the amount of broadening that takes place. Further experimental work on this problem is required.

If one is interested in only measuring the total concentration of helium in very narrow distributions then considerable simplification of the problem is achieved. In this case, Eq. (2) becomes a function of x' only and integration can be eliminated, resulting in a simple evaluation of N and the number of helium atoms.

VI. CONCLUSIONS

It has been demonstrated that the ^{3}He$(d,p)^4$He reaction can be used for profiling helium in solids.

Resolution-enhancement techniques result in spacial resolution of about 6000 Å when probing with a deuteron beam. The resolution will be about a factor of 5 better in the case of probing deuterons with ^{3}He, since the stopping power for helium is that much higher. Corrections for beam broadening and energy straggling should help to give considerable improvement to the resolution.

It is worth mentioning that spatial resolution of 300 Å for helium distributions and 200 Å for hydrogen distributions would seem to be possible if one works with high-energy heavy-particle beams. For example, the reaction ^{1}H(^{19}F, $\alpha\gamma$)^{16}O has recently been used for profiling hydrogen in silicate materials.[4] Anomalous 100%-broadened half-widths were observed in their case but were attributed to diffusion effects. Use of a fluorine probing beam requires tandem accelerator energies in the range of 16 to 18 MeV, since the center-of-mass energy will be much higher. As pointed out in Ref. 4, lower energies could be used with the ^{1}H(^{15}N, $\alpha\gamma$) ^{12}C reaction. Likewise, 4-MeV boron beams may yield lower-limit resolution of about 300 Å for helium profiling with the ^{4}He(^{10}B, n)^{13}N reaction. Perturbations from the high-energy heavy-ion beam on the distributions would, in any case, have to be carefully monitored.

ACKNOWLEDGMENTS

We thank Dr. R. E. McDonald and Dr. A. Taylor for their suggestions and discussions in this work. Dr. K. L. Merkle and Dr. H. Wiedersich also participated in discussions and comments on the manuscript. We are grateful to Professor S. S. Hanna for making available the Stanford 3-MeV accelerator that was used for our implants.

---

*Work supported by the U. S. Atomic Energy Commission and the Lockheed Independent Research Fund.

[1]A. G. Pieper, R. B. Theus, L. S. August, and F. A. Smidt, Bull. Am. Phys. Soc. 18, 578 (1973).

[2]W. R. Phillips and F. H. Read, Proc. Phys. Soc. Lond. 81, 1 (1963).

[3]P. H. Barber and W. R. Phillips, Proc. Phys. Soc. Lond. 86, 379 (1965).

[4]D. A. Leich and T. A. Tombrello, Nucl. Instrum. Methods 108, 67 (1973).

[5]T. W. Bonner, J. P. Conner, and A. B. Lillie, Phys. Rev. 88, 473 (1952).

[6]C. F. Williamson, J. P. Boujot, and J. Picard, Centre D'Etudes Nucléaires de Saclay Report No. CEA-R 3042 (1966) (unpublished).

[7]H. E. Schiott, Mat. Fys. Medd. Dan. Vidensk. Selsk. 35, No. 9 (1966).

[8]J. Lindhard, M. Scharff, and H. E. Schiott, Mat. Fys. Medd. Dan. Vidensk. Selsk. 33, No. 14 (1963).

[9]*American Institute of Physics Handbook*, 3rd ed., edited by D. E. Gray (McGraw-Hill, New York, 1972), Sec. 8, p. 176.

[10]J. F. Ziegler and J. W. Baglin, J. Appl. Phys. 42, 7031 (1971).

[11]Charged Particle Cross Sections, Los Alamos Scientific Laboratories, University of California Report No. LA-2014 (1956) (unpublished).

[12]C. Tschalär, Nucl. Instrum. Meth. 61, 141 (1968).

[13]W. T. Scott, Rev. Mod. Phys. 35, 231 (1963).